TR - O - 0038

48

BER Performance of Anti-Multipath Modulation Scheme PSK-VP and its Optimum Phase-Waveform

Hitoshi TAKAI

1991. 3. 31.

ATR光電波通信研究所

Abstract

This paper proposes a new anti-multipath modulation scheme which the author calls PSK-VP (Phase Shift Keying with Varied Phase) in which a varied phase-waveform is redundantly imposed on the DPSK timeslot. The relationship between the phase-waveform and BER is discussed by using an analytical approach based on special diversity with a continuous branch. A formula-type BER expression is obtained by the analytical approach and shows the optimum phase-waveform condition. A convex phase-waveform asymptotically satisfies the optimum phase-waveform condition as its phase shift peak is increased. 'PSK-VP with a convex phase-waveform' raises the delay difference upper limit to almost 1 symbol and shows an excellent BER for a multipath fading whose delay differences are less than the upper limit. A numerical evaluation also confirms the above results and additionally shows that 4-ary PSK-VP can nearly double the upper limit as measured in bits, which is about 1.7 bits for the convex phase-waveform.

The author was with ATR Optical and Radio Communications Research Laboratories, Seika-cho, Soraku-gun, Kyoto 619-02, Japan. He is now with Kansai Information and Communications Research Laboratory, Matsushita Electric Industrial Co., Ltd., Moriguchi, Osaka 570, Japan.

Contents

List of Figures

I INTRODUCTION

High-speed digital mobile communications are severely affected by the frequency-selective fading caused by multipath with various time delays[1]–[3], which characterizes their radio channels. Severe intersymbol interference caused by the frequency-selective fading greatly degrades the BER (Bit Error Rate)[4], and consequently limits the maximum transmission data rate.

To combat the BER degradation, various anti-multipath modulation schemes, in which a redundant phase/amplitude transition is imposed on a basic conventional modulation, have been proposed[5]–[9]. In general, these modulation schemes are characterized by *hardware simplicity* with no adaptive process, and an *excellent BER* for a multipath fading whose delay differences are less than a certain value (hereafter, called *delay difference upper limit*). For example, the upper limit of DSK[6] is less than 0.5 bits.

Raising the delay difference upper limit, which is equivalent to raising the usable bit-rate, is an important problem for such anti-multipath modulation schemes, because the limit is rather low for applications to various propagation environments or applications at a higher bit-rate. The choice of the basic modulation and how the redundancy should be imposed determine the upper limit. By choosing DPSK as the basic modulation, PSK-RZ[7] with amplitude redundancy, SPSK[8] and MC-PSK[9] with redundant phase-jump have successfully extended the limit. This is because M-ary versions of the above can significantly extend the limit as measured in bits. However, optimization for redundancy to extend the limit has not been discussed.

In this paper, the author proposes 'PSK-VP with a *convex phase-waveform*' as an answer to the problem. PSK-VP (Phase Shift Keying with Varied Phase)[10] is defined as a generic name for modulation schemes in which a *varied phase-waveform* is redundantly imposed on the DPSK timeslot. Then, the optimum shape of the redundant phase-waveform is investigated.

PSK-VP (in particular, 2- and 4-ary PSK-VP, i.e., BPSK-VP and QPSK-VP are dealt with in this paper) is characterized using an analytical approach and a numerical evaluation. The analytical approach reveals the major BER features, in particular, the relationship between the BER and the phase-waveform through a *formula-type* BER expression, and determines the optimum shape of the phase-waveform through an optimum phase-waveform condition derived from the BER expression. The numerical evaluation verifies the above results.

The analytical approach is based on diversity. Though similar unique DSK analysis

was done by Ariyavisitakul *et al.*[6], extensions are required because the diversity for PSK-VP is a special type with a *continuous* branch and the previous analysis cannot estimate the changing of the BER to a delay difference. Using the analytical approach, not only is the improvement mechanism (a kind of path diversity) clarified, but we also obtain the formula-type BER expression.

The analytical approach is done mainly for two-ray Rayleigh fading, then extended for general L-ray Rayleigh fading. All major PSK-VP characteristics are revealed for two-ray Rayleigh fading, and they or their reasonable extensions are also obtained for L-ray Rayleigh fading.

The numerical evaluation is based on an analysis method for a quadratic detector using a characteristic function, which was studied by Kac and Siegert[11] and Turin[12], and was also applied to analyze DSK[6]. The numerical evaluation, which is rearranged to analyze PSK-VP, is mainly done to verify the results of the analytical approach with several approximations and assumptions, and to reveal other PSK-VP characteristics which the analytical approach can not deal with.

The numerical evaluation nicely confirms the excellent performance of PSK-VP with a convex phase-waveform estimated by the analytical approach and additionally reveals a robust feature for rapid fading.

II PSK-VP SCHEME

II.1 PSK-VP Signal

In PSK-VP, a varied phase-waveform $\phi(\epsilon)$ is redundantly imposed on the DPSK time-

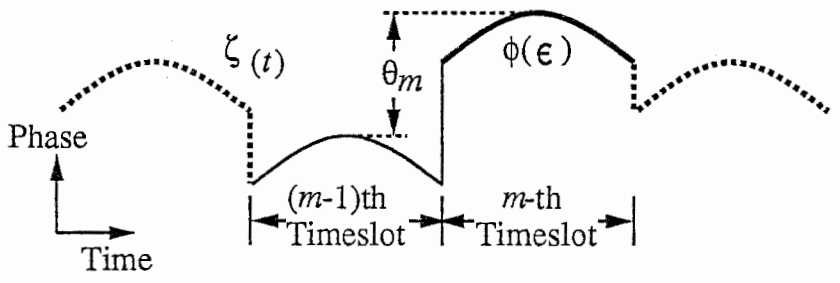

Figure II1: PSK-VP signal phase (an example for convex phase-waveform).

slot (Fig.II1). The PSK-VP signal phase $\zeta(t)$ is expressed as

$$\zeta(t) = \zeta(\epsilon + mT) = \phi(\epsilon) + \vartheta_m \quad ; m = \cdots, -2, -1, 0, 1, 2, \cdots \ , \tag{II1}$$

where ϵ=$t-mT$ ($0 \leq \epsilon < T$, T:symbol length, i.e., timeslot). The phase difference between the $(m-1)$th timeslot and the m-th timeslot:

$$\theta_m = \vartheta_m - \vartheta_{m-1} \tag{II2}$$

bears the m-th M-ary data. Though various methods to map the data into θ_m can be considered, in this paper, it takes 0 (*mark*) or π (*space*) for 2-ary PSK-VP (BPSK-VP) and 0 (*mark-mark*), $\pi/2$ (*space-mark*), π (*space-space*) or $3\pi/2$ (*mark-space*) for 4-ary PSK-VP (QPSK-VP) which are conventionally mapped according to the Gray encoding. (Of course, symmetrical mapping[13], i.e., $\pm\pi/2$ for BPSK-VP and $\pm\pi/4$, $\pi\pm\pi/4$ for QPSK-VP is also possible. However, because the following analysis is exactly the same when the intersymbol interference due to band-limitation is ignored, in this paper, only the conventional asymmetric mapping is dealt with.)

Then, if the band-limitation effect is ignored, the complex envelope of PSK-VP signal is expressed as

$$v(t) = e^{j\zeta(t)} \ . \tag{II3}$$

Hereafter, j denotes $\sqrt{-1}$.

II.2 PSK-VP Detection Process

PSK-VP detection is carried out with a differential detector (Fig.II2). If a complex envelope of received signal is expressed as $z_1(t)$, the complex envelope $z_2(t)$ of the delayed signal will be expressed as

$$z_2(t) = z_1(t-T) \cdot e^{-j\psi} \ , \tag{II4}$$

where ψ denotes the detection phase, which takes 0 for BPSK-VP and $\pm\pi/4$ according to the I/Q-axis for QPSK-VP. The detected signal $d(t)$, i.e., the baseband component of the product of $z_1(t)$ and $z_2(t)$, results in

$$d(t) = \frac{1}{4}(z_1 z_2^* + z_1^* z_2) \ . \tag{II5}$$

Hereafter, * denotes complex conjugate. The output signal $Q(t)$ of the postdetection filter with impulse response $h(t)$ results in

$$Q(t) = h(t) \otimes d(t) \ , \tag{II6}$$

where $\otimes$ denotes convolution. Then, the sampled signal q of $Q(t)$ by clock timing t_s recovered by $Q(t)$ itself, is decoded to *mark/space* by its polarity.

III ANALYTICAL APPROACH

III.1 Detection Output for Two-Ray Model

First, we consider a detection output for a two-ray (D- and U-wave) model with a delay difference τ, whose waves are subjected to Rayleigh fading. By representing each fading with multiplicative noise $s_1(t)$ or $s_2(t)$, which includes the phase rotation due to the delay τ and is a zero-mean complex gaussian random process, we can express the received signal $z_1(t)$ without extraneous noise as

$$z_1(t) = s_1(t)v(t) + s_2(t)v(t-\tau) \ . \tag{III1}$$

Transforming t to ε by $\varepsilon{=}t{-}mT{-}\tau$ and defining μ as

$$\mu = \begin{cases} 1 & \text{for BPSK-VP} \\ \dfrac{1}{\sqrt{2}} & \text{for QPSK-VP} \end{cases} \ , \tag{III2}$$

and $a_m(=\pm 1)$ as the m-th transmitted binary data for the detection axis, from Appendix A, we can derive the m-th timeslot detected signal $d_m(\varepsilon)$ ($\equiv d(\varepsilon{+}mT{+}\tau)$; $-\tau{\le}\varepsilon{<}T{-}\tau$) for slow fading and $0{\le}\tau{<}T$, separately for the following two regions (Fig.III1).

1) Region:a $0 \le \varepsilon < T - \tau$ (will vanish for $\tau{\ge}T$)

$$d_m(\varepsilon) = \frac{1}{2}\mu a_m \mid s_1 e^{j\phi(\varepsilon+\tau)} + s_2 e^{j\phi(\varepsilon)} \mid^2 \tag{III3}$$

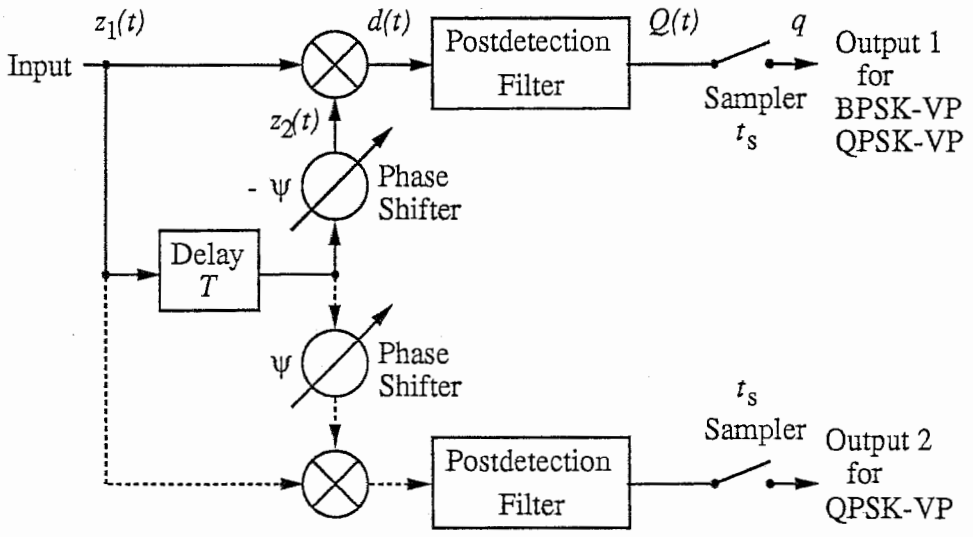

Figure II2: Detection process for PSK-VP (block diagram of differential detector).

In this region, the polarity of the detected signal, which is hereafter called the '*effective* detected signal', is always correct.

2) Region:b $-\tau \leq \varepsilon < 0$ (will vanish for τ=0)

$$d_m(\varepsilon) = \frac{\mu}{2}(a_m \mid s_1 \mid^2 + a_{m-1} \mid s_2 \mid^2)$$

$$+ \cos(\frac{\theta_m + \theta_{m-1}}{2} + \psi)\Re[s_1 s_2^* \exp j(\phi(\varepsilon+\tau) - \phi(\varepsilon+T) + \frac{\theta_m + \theta_{m-1}}{2})] \,, \qquad \text{(III4)}$$

where $\Re[\cdot]$ denotes real part.

In this region, the polarity of the detected signal, which is called the '*ineffective* detected signal' hereafter, is not always correct.

III.2 Diversity Model for PSK-VP

The effective detected signal behaves as if the received signal were subjected to frequency-nonselective fading expressed by the linearly combined multiplicative noise $s_1 e^{j\phi(\varepsilon+\tau)} + s_2 e^{j\phi(\varepsilon)}$,

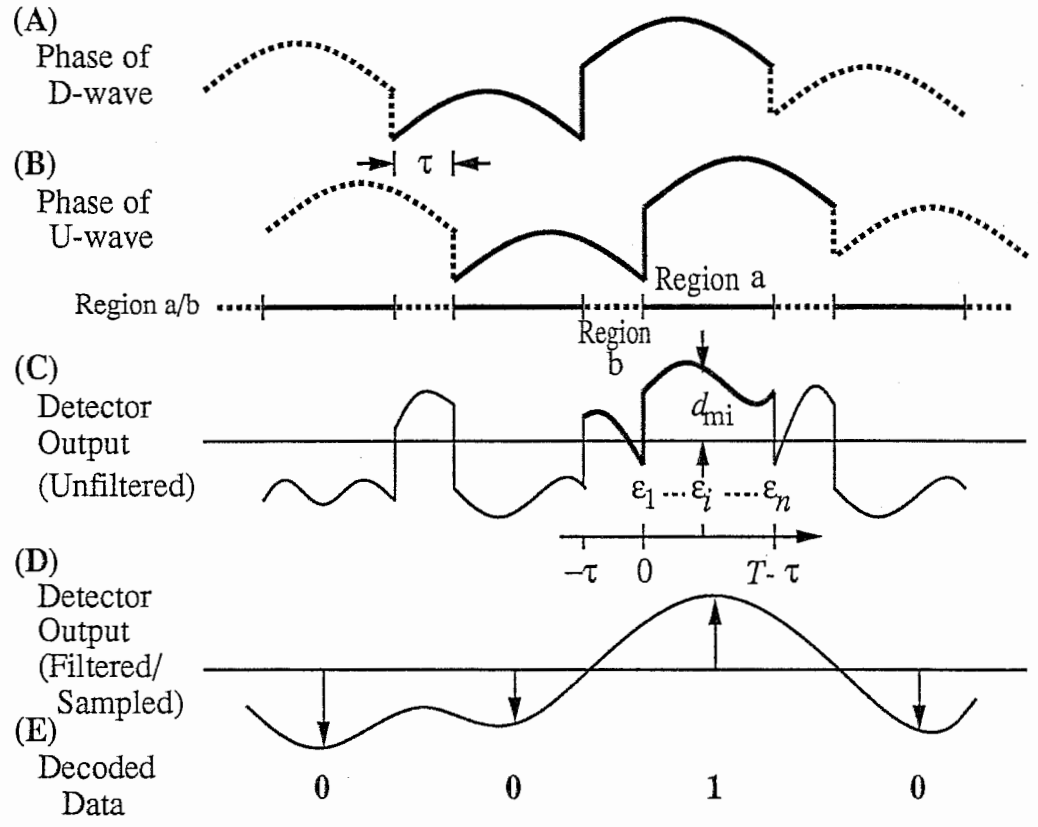

Figure III1: Detection output for two-ray model.

which varies with ε. Namely, different kinds of detected signals are obtained along Region:a (Fig.III1(C)). Then, a diversity effect is expected, because the different kinds of detected signals are combined by convolution with the impulse response of the postdetection filter (Fig.III1(D)). The diversity seems to have a *continuous* branch.

To analyze the diversity with a continuous branch, first, we divide Region:a into n pieces which are sufficiently small. On the i-th piece position ε_i:

$$\varepsilon_i = (T-\tau)(i-1)/n \qquad ; \ i = 1, 2, \cdots, n \ , \tag{III5}$$

the effective detected signal d_{mi} is rewritten as

$$d_{mi} \equiv d_m(\varepsilon_i) = \frac{1}{2}\mu a_m \mid s_1 e^{j\phi_{1i}} + s_2 e^{j\phi_{2i}} \mid^2 \qquad ; \ i = 1, 2, \cdots, n \tag{III6}$$

by defining

$$\begin{cases} \phi_1(\varepsilon) &= \phi(\varepsilon + \tau) \\ \phi_2(\varepsilon) &= \phi(\varepsilon) \end{cases} , \tag{III7}$$

and abbreviating $\phi_l(\varepsilon_i)$ to ϕ_{li} ($l = 1, 2$ and i=1,2,$\cdots$,n).

The equivalent multiplicative noise ν_i, which represents the *frequency-nonselective* fading yielding the same detected signal as d_{mi} in Eq.(III6), is expressed as the following

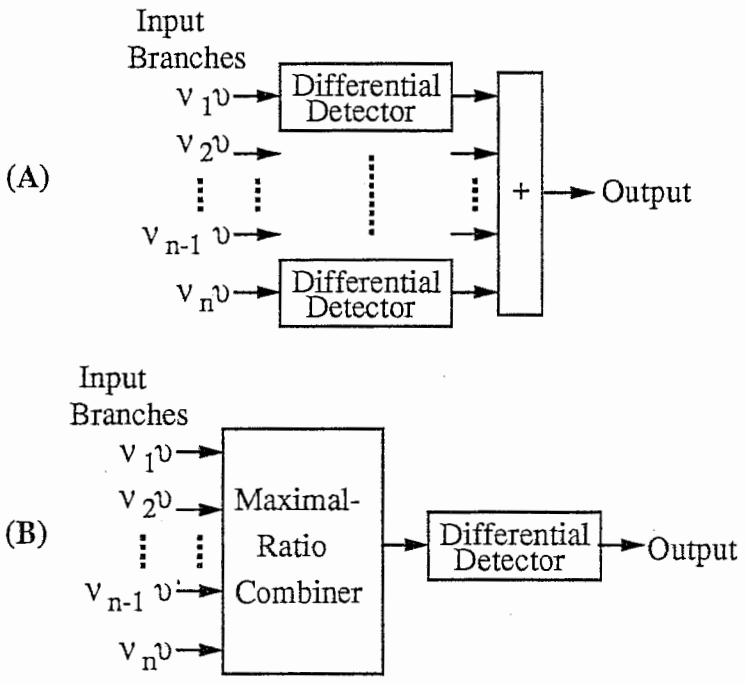

Figure III2: Diversity models for PSK-VP.

linear combination of s_1 and s_2

$$\nu_i = s_1 e^{j\phi_{1i}} + s_2 e^{j\phi_{2i}} \quad ; \; i = 1, 2, 3, \cdots, n \; . \tag{III8}$$

Consequently, ν_i is also a zero-mean complex gaussian random process. Then, as shown in Fig.III2(A), PSK-VP in multipath fading is considered to be equivalent to DPSK with n-branch postdetection combining diversity whose branches are subjected to the above frequency-nonselective fadings ν_i, because the postdetection filter combines the effective detected signals d_{mi}. Such a combining method, which is known as square-law combining, is optimum without knowledge of the instantaneous branch SNR[14].

For further analysis, the following approximations and assumptions will be used.

Approx.1) Approximate the postdetection diversity with the square-law combiner (Fig.III2(A)) to a predetection diversity with the maximal-ratio combiner (Fig.III2(B)).

It is difficult to obtain a formula-type solution for the diversity in Fig.III2(A) because of correlation between the branches. The diversity in Fig.III2(B), which is optimum though requiring perfect knowledge of the branches, has a similar BER performance at low error-rates[14] and is easily analyzed.

Assum.1) Each effective detected signal d_{mi} is equally combined.

Assum.2) The output SNR of the maximal-ratio combiner is proportional to the normalized interval of Region:a, i.e., $1-\tau/T$.

Combining d_{mi} depends on the postdetection filter and the sampling timing. Assumptions 1 and 2 imply an integrate-and-dump postdetection filter with correct timing.

Approx.2) Ignore the ineffective detected signal.

We use numerical evaluation to investigate the effect of the ineffective detected signal.

Although BER calculated from the above simplified diversity may include absolute error, the analysis is still meaningful for obtaining physical views and estimating *relative* performance; for example, comparisons between BER performance for various phase-waveforms ϕ or changing BER to SNR.

III.3 Condition for Diversity Effect

According to Assumptions 1 and 2, and by considering that the maximal-ratio combiner causes the output SNR to equal the sum of input SNRs, we find that each input branch SNR is proportional to $(1-\tau/T)/n$. Consequently, from Eq.(III8), the complex multi-

plicative process γ_i on each branch normalized to rms noise, is expressed as

$$\gamma_i = \sqrt{\frac{1-\tau/T}{n}}\frac{\nu_i}{\sqrt{N}} = \frac{\sqrt{\frac{1-\tau/T}{n}}(s_1 e^{j\phi_{1i}} + s_2 e^{j\phi_{2i}})}{\sqrt{N}} \quad ; \; i = 1, 2, 3, \cdots, n \; , \tag{III9}$$

where N denotes noise power. Then, the average BER $\hat{P}_e$ of the diversity in Fig.III2(B) for slow fading is simply expressed as[6][14]

$$\hat{P}_e = \frac{1}{2\det(\boldsymbol{I} + \boldsymbol{X})} \; , \tag{III10}$$

where $\boldsymbol{I}$ denotes an $n \times n$ unit matrix and $\boldsymbol{X}$ denotes an $n \times n$ covariance matrix of γ_i. Furthermore, if the fadings of the D- and U-waves are uncorrelated, through direct calculation, by using matrix $\boldsymbol{X}_0$, matrix $\boldsymbol{X}$ is expressed as

$$\boldsymbol{X} = \frac{(1-\frac{\tau}{T})\Gamma}{n}\boldsymbol{X}_0 \; , \tag{III11}$$

whose ik-element X_{0ik} is

$$X_{0ik} = \frac{\rho}{1+\rho}e^{j(\phi_{1i}-\phi_{1k})} + \frac{1}{1+\rho}e^{j(\phi_{2i}-\phi_{2k})} \quad ; \; i, k = 1, 2, \cdots, n \; , \tag{III12}$$

where ρ ($\equiv\langle|s_1|^2\rangle/\langle|s_2\ |^2\rangle$) denotes average DUR (D-wave to U-wave level ratio), Γ ($\equiv(\langle|s_1|^2\rangle+\langle|\ s_2|^2\rangle)/N$) denotes average SNR per bit, and $\langle\cdot\rangle$ denotes ensemble average. Note that Eq.(III10) is originally derived for 2-ary DPSK with diversity, however, it is also (approximately) valid for the Gray-code mapped 4-ary DPSK with diversity when Γ is the average SNR *per bit* (i.e., 4-ary DPSK requires a 3dB better *SNR* for the same BER compared with 2-ary DPSK)[15].

From Eq.(III12), second- and third-order minor determinants r_2, r_3 of matrix $\boldsymbol{X}_0$ are calculated as

$$\begin{cases} r_2 &= \dfrac{\rho}{(1+\rho)^2}(e^{-j\Phi_{k+1}} - e^{-j\Phi_k})(e^{j\Phi_{i+1}} - e^{j\Phi_i}) \\ r_3 &= 0 \end{cases} \tag{III13}$$

by defining

$$\Phi(\varepsilon, \tau) \equiv \phi_1(\varepsilon) - \phi_2(\varepsilon) = \phi(\varepsilon + \tau) - \phi(\varepsilon) \tag{III14}$$

and abbreviating $\Phi(\varepsilon_i, \tau)$ to Φ_i (i=1,2,$\cdots$,n). Equation(III13) results in rank$\boldsymbol{X}$=rank$\boldsymbol{X}_0\leq$2 and the n-branch diversity can effectively function as second-order diversity. The order *two* is derived from obtaining n branches through the linear combination of *two* independent fadings. The diversity can be regarded as a path diversity.

Then, from $r_2 \neq 0$ in Eq.(III13), the condition for obtaining the diversity effect is expressed as

$$\exists \varepsilon, \delta \in \{(\varepsilon, \delta) \mid 0 \leq \varepsilon < \varepsilon + \delta < T - \tau\}$$
$$\Phi(\varepsilon + \delta, \tau) \neq \Phi(\varepsilon, \tau) \quad : \bmod 2\pi \ . \tag{III15}$$

The diversity condition is easily satisfied for a certain τ by introducing discontinuity or variation into Φ by imposing a redundant phase-jump or a phase-variation to phase-waveform ϕ (cf. Fig.III3). However, the choice of the redundancy must be carefully examined to determine whether the condition is satisfied for all τ in $0<\tau<T$ (then, the delay difference upper limit is raised to 1 timeslot), where, from Eq.(III15) itself, the diversity effect can be obtained. As shown in subsection F, the redundant phase-jump (stepped phase-waveform) has an adverse effect on raising the upper limit.

III.4 Major BER Features of PSK-VP Subjected to Two-Ray Rayleigh Fading

Finally, we obtain BER expression P_e as the continuous-branch diversity by considering the limit of BER $\hat{P}_e$ as the n-branch (discrete) diversity when $n \to \infty$ (Appendix B and C), i.e.,

$$P_e = \lim_{n \to \infty} \hat{P}_e = \frac{1}{2\{\Gamma^2 (1 - \frac{\tau}{T})^2 \frac{\rho}{(1+\rho)^2} (1 - \mid F(\tau) \mid^2) + \Gamma(1 - \frac{\tau}{T}) + 1\}} \ , \tag{III16}$$

where

$$F(\tau) \equiv \frac{1}{T - \tau} \int_0^{T-\tau} e^{j\Phi(\varepsilon, \tau)} d\varepsilon \quad ; \ 0 \leq \mid F(\tau) \mid \leq 1 \ . \tag{III17}$$

Equation(III16) provides considerable information about PSK-VP BER characteristics. First, we investigate the major PSK-VP BER features.

1) For Frequency-Selective Fading $(0 < \tau < T, 0 < \rho < \infty)$

The BER is remarkably improved proportional to the square of the SNR Γ for high SNR by the term including Γ^2 in the denominator, where the condition $|F(\tau)|<1$ (which is equivalent to the diversity condition Eq.(III15)) is satisfied.

2) For Frequency-Nonselective Fading $(\tau = 0$ or $\rho = 0$ or $\rho = \infty)$

The term including Γ^2 disappears, because $F(0)=1$ ($\tau=0$ results in $\Phi \equiv 0$ from Eq.(III14)) or $\rho/(1+\rho)^2=0$ ($\rho=0$ or ∞). Consequently, Eq.(III16) becomes

$$P_e = \frac{1}{2(\Gamma + 1)} \ , \tag{III18}$$

which is identical to conventional DPSK[15] (The DPSK BER is also obtained from Eq.(III16) itself, because ϕ=const. also results in $\Phi\equiv 0$.).

3) QPSK-VP vs. BPSK-VP

The same τ measured in symbol lengths shows almost the same performance except for a slight BER degradation (3dB in SNR). However, as measured in bit lengths, QPSK-VP is expected to double the delay difference upper limit.

III.5 Ideal Boundary and Optimum Condition for Phase-Waveform

By transforming Eq.(III16), we find that

$$P_e \geq \frac{1}{2\{\frac{(1-\tau/T)\Gamma}{2}+1\}^2} . \tag{III19}$$

The lower limit shows an ideal boundary of BER improved by the diversity effect. The ideal boundary implies that the diversity effect can be obtained over $0<\tau<T$. Namely, by choosing an appropriate phase-waveform, PSK-VP can raise the delay difference upper limit by 1 symbol, which is essentially derived from the existence of Region:a.

The condition for equality in Eq.(III19) is

$$\mid F(\tau) \mid \equiv \mid \frac{1}{T-\tau}\int_0^{T-\tau} e^{j\Phi(\varepsilon,\tau)}d\varepsilon \mid = 0 , \tag{III20}$$

and

$$\rho = 1 \quad \text{(i.e., D- and U-waves have same level)} . \tag{III21}$$

In particular, Eq.(III20) shows optimum condition for phase-waveform ϕ through Φ, where the maximum diversity improvement can be achieved.

For all τ in $0<\tau<T$, no function Φ strictly satisfies the optimum phase-waveform condition in Eq.(III20). However, the strictly monotone increasing/decreasing (as to ε for any τ) function $\Phi(\varepsilon,\tau)$ can asymptotically satisfy the optimum phase-waveform condition by increasing its range. That is, a convex phase-waveform ϕ can asymptotically satisfy the optimum phase-waveform condition by increasing its peak, because the choice of a strictly monotone function for Φ is equivalent to the choice of a convex function for ϕ as follows:

$$\forall \varepsilon,\delta,\tau \in \{(\varepsilon,\delta,\tau) \mid 0 \leq \varepsilon < \varepsilon+\delta < T-\tau, 0<\tau<T\}$$

$$\Phi(\varepsilon+\delta,\tau)-\Phi(\varepsilon,\tau)$$

$$= \{\phi(\tau+\varepsilon+\delta)-\phi(\tau+\varepsilon)\}-\{\phi(\varepsilon+\delta)-\phi(\varepsilon)\}$$

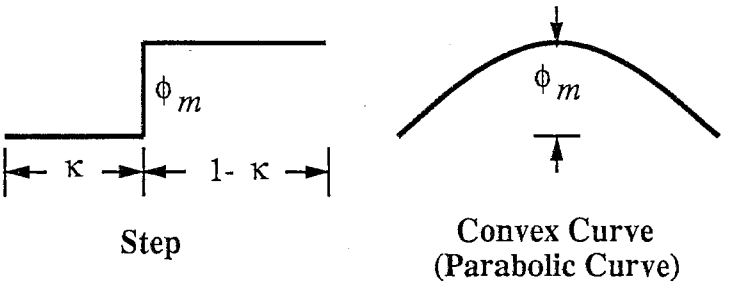

Figure III3: Stepped and Convex (Parabolic) phase-waveforms.

$$\begin{cases} > 0 & \text{for strictly monotone increasing} \\ < 0 & \text{for strictly monotone decreasing} \end{cases} . \tag{III22}$$

The above relationship also shows that a convex phase-waveform ϕ guarantees satisfying the diversity condition in Eq.(III15) for any τ in $0<\tau<T$.

Of course, excluding a stepped phase-waveform, which adversely affects raising the delay difference upper limit (subsection F) and tends to corrupt the eye-pattern due to the existence of the phase discontinuity in the timeslot for bandlimitation, there are more complicated phase-waveform candidates to satisfy Eq.(III20) asymptotically, for example, (continuous) phase-waveforms with several peaks. However, a convex phase-waveform is the most reasonable as follows. If ϕ is a continuous (differentiable or piecewise differentiable) function, by differentiating Eq.(III14) as to ε,

$$\frac{\partial\Phi(\varepsilon,\tau)}{\partial\varepsilon} = \phi'(\varepsilon+\tau) - \phi'(\varepsilon) \tag{III23}$$

is obtained. Then, in Eq.(III23), by considering that $\phi'(\varepsilon+\tau)$ and $\phi'(\varepsilon)$ designate instantaneous angular frequency deviations from the carrier frequency at $\varepsilon+\tau$ and ε in the timeslot, to obtain spectrum compactness, the smaller $\partial\Phi/\partial\varepsilon$ is, the better. The choice of strictly monotone increasing/decreasing function for Φ (as to ε), i.e., a convex phase-waveform ϕ is the best way to minimize $|F(\tau)|$ in Eq.(III20) effectively, while keeping the differential coefficient $\partial\Phi/\partial\varepsilon$ small.

III.6 Examples for Typical Phase-Waveforms

For example, we will compare BER performance for the typical phase-waveforms, which are stepped and parabolic (an example of convex) as shown in Fig.III3.

1) Stepped Phase-Waveform

This is identical to SPSK[8], and the specific case of κ=0.5 is identical to MC-PSK[9]. ϕ and Φ are expressed as

$$\phi(\epsilon) = \begin{cases} 0 & (0 \leq \epsilon < \kappa T) \\ \phi_m & (\kappa T \leq \epsilon < T) \end{cases} \quad ; \ 0 < \kappa < 1 \tag{III24}$$

$$\Phi(\varepsilon, \tau) = \begin{cases} 0 & (0 \leq \varepsilon < \kappa T - \tau \text{ or } \kappa T \leq \varepsilon < T - \tau) \\ \phi_m & (\kappa T - \tau \leq \varepsilon < \kappa T) \end{cases} . \tag{III25}$$

If $\tau \geq \tau_m = \max(\kappa T, T - \kappa T)$, because $\Phi \equiv \phi_m$ is derived for $0 \leq \varepsilon < T - \tau$, Eq.(III15) is not satisfied and the diversity improvement is lost. Namely, the delay difference upper limit is reduced to $\tau_m (< T$. See Fig.III4).

2) Parabolic Phase-waveform

ϕ and Φ are expressed as

$$\phi(\epsilon) = -4 \cdot \frac{\phi_m}{T^2} \cdot \epsilon(\epsilon - T) \tag{III26}$$

$$\Phi(\varepsilon, \tau) = -\frac{8\phi_m \tau}{T^2} \varepsilon + \phi(\tau) . \tag{III27}$$

By calculating Eq.(III17), $|F(\tau)|$ is expressed as

$$| F(\tau) | = \frac{| \sin \phi(\tau) |}{\phi(\tau)} . \tag{III28}$$

At all τ in $0 < \tau < T$, $|F(\tau)|$ approaches zero and BER asymptotically approaches the ideal boundary as the phase-shift peak ϕ_m is increased, because the numerator of Eq.(III28) is bounded (Fig.III5).

III.7 Extension to L-Ray Model

The analytical approach can be extended to general L-ray model and reasonably-extended results of the two-ray model are derived for the L-ray model. That is, also for the L-ray model, the optimum phase-waveform condition (Eq.(III20)) is essentially the same, and a convex phase-waveform is considered to be optimum to obtain the maximum BER improvement. The outline is shown as follows.

First, the received signal $z_1(t)$ in Eq.(III1) is rewritten as

$$z_1(t) = \sum_{l=1}^{L} s_l(t) v(t - \tau_l) , \tag{III29}$$

where $s_l(t)$ denotes multiplicative noise representing the fading of the l-th path and τ_l denotes excess delay of the l-th path. Then, redefining τ as the maximum of τ_l and

assuming that the minimum of τ_l is zero, transforming t to ε by ε=$t-mT-\tau$, and using μ in Eq.(III2), the m-th timeslot detected signal $d_m(\varepsilon)$ in Eq.(III3) for slow fading and $0\leq\tau<T$ in the region of $0\leq\varepsilon<T-\tau$ (corresponding to Region:a) is rewritten as

$$d_m(\varepsilon) = \frac{1}{4}\mu a_m \mid \sum_{l=1}^{L} s_l e^{j\phi(\varepsilon+\tau-\tau_l)} \mid^2 , \tag{III30}$$

as shown in Appendix A. In this region, the detected signal polarity is always correct, i.e., *effective*, the same as in the case of the two-ray model.

Dividing the effective region into n pieces, on the n-th piece position ε_i (Eq.(III5)), the effective detected signal d_{mi} in Eq.(III6) is rewritten as

$$d_{mi} \equiv d_m(\varepsilon_i) = \frac{1}{4}\mu a_m \mid \sum_{l=1}^{L} s_l e^{j\phi_{li}} \mid^2 \quad ; \; i = 1, 2, \cdots, n \tag{III31}$$

by extending the definition Eq.(III7) as

$$\phi(\varepsilon + \tau - \tau_l) = \phi_l(\varepsilon) \quad ; \; l = 1, 2, \cdots, L , \tag{III32}$$

and abbreviating $\phi(\varepsilon_i+\tau-\tau_l)$ to ϕ_{li} (l=1,2,$\cdots$,L and i=1,2,$\cdots$,n). Consequently, because the multiplicative noises ν_i corresponding to d_{mi} are rewritten as $\nu_i = \sum_{l=1}^{L} s_l e^{j\phi_{li}}$, the normalized multiplicative noise γ_i in Eq.(III9) is rewritten as

$$\gamma_i = \sqrt{\frac{1-\tau/T}{n}}\frac{\nu_i}{\sqrt{N}} = \frac{\sqrt{\frac{1-\tau/T}{n}}\sum_{l=1}^{L} s_l e^{j\phi_{li}}}{\sqrt{N}} \quad ; \; i = 1, 2, 3, \cdots, n . \tag{III33}$$

If each fading of the L rays is uncorrelated, matrix $\boldsymbol{X}$ is also expressed by using matrix $\boldsymbol{X}_0$ (Eq.(III11)), however, its ik-element X_{0ik} is rewritten as

$$X_{0ik} = \sum_{l=1}^{L} \xi_l e^{(\phi_{li}-\phi_{lk})} \quad ; \; i, k = 1, 2, \cdots, n \tag{III34}$$

by defining

$$\begin{cases} \xi_l &= \langle \mid s_l \mid^2 \rangle / \sum_{k=1}^{L} \langle \mid s_k \mid^2 \rangle \quad ; \; l = 1, 2, \cdots, L \\ \Gamma &= \sum_{k=1}^{L} \langle \mid s_k \mid^2 \rangle / N \end{cases} , \tag{III35}$$

where ξ_l denotes the l-th ray power ratio to total signal power and Γ denotes average SNR.

In this case, because rank$\boldsymbol{X}$=rank$\boldsymbol{X}_0\leq L$ (cf. Appendix C), the diversity can effectively function as a maximum of L-th order diversity, which is easily understood by considering that the diversity is a kind of path diversity with L independent-fading paths.

The choice of a convex phase-waveform ϕ is also valid for the L-ray model to obtain the maximum order diversity effect (i.e., rank$\boldsymbol{X}$=rank$\boldsymbol{X}_0$=L). A convex phase-waveform ϕ is verified to guarantee rank$\boldsymbol{X}$=rank$\boldsymbol{X}_0$=L by a reductio ad absurdum as shown in Appendix D.

Then, if rank$\boldsymbol{X}$=rank$\boldsymbol{X}_0$=L, as shown in Appendix B, an approximation of BER P_e

$$P_e = \lim_{n\to\infty} \hat{P}_e \approx \frac{1}{2\Gamma^L(1-\frac{\tau}{T})^L \prod_{k=1}^{L} \xi_k \det \boldsymbol{F}} \tag{III36}$$

is obtained for high SNR Γ by using $L\times L$ matrix $\boldsymbol{F}$ whose $\alpha\beta$-element $F_{\alpha\beta}$ is expressed as

$$F_{\alpha\beta}(\tau) = \frac{1}{T-\tau}\int_0^{T-\tau} e^{j\Phi_{\alpha\beta}(\varepsilon,\tau)}d\varepsilon \quad ;\ \alpha,\beta = 1,2,\cdots,L\ , \tag{III37}$$

by extending the definition Eq.(III14) as

$$\Phi_{\alpha\beta}(\varepsilon,\tau) \equiv \phi_\beta(\varepsilon) - \phi_\alpha(\varepsilon) = \phi(\varepsilon+\tau-\tau_\beta) - \phi(\varepsilon+\tau-\tau_\alpha) \quad ;\ \alpha,\beta = 1,2,\cdots,L\ . \tag{III38}$$

By the term of Γ^L in the denominator, the BER is remarkably improved proportional to the L-th power of the SNR Γ.

As shown in Appendix E, the improved BER in Eq.(III36) has the following lower limit:

$$P_e \geq \frac{1}{2\Gamma^L(1-\frac{\tau}{T})^L \frac{1}{L^L}}\ . \tag{III39}$$

The lower limit is the ideal boundary of improved BER for the L-ray Rayleigh fading. The equality condition in Eq.(III39) is

$$|\ F_{\alpha\beta}(\tau)\ | \equiv \left|\ \frac{1}{T-\tau}\int_0^{T-\tau} e^{j\Phi_{\alpha\beta}(\varepsilon,\tau)}d\varepsilon\ \right| = 0 \quad ;\ \alpha\neq\beta\ ,\ \alpha,\beta = 1,2,\cdots,L\ , \tag{III40}$$

and

$$\forall\xi_k = \frac{1}{L} \quad \text{(i.e., each arriving wave has the same level)}\ . \tag{III41}$$

The above results are reasonable extensions of the optimum condition for the two-ray model in Eq.(III20) and Eq.(III21). In particular, Eq.(III40) is the optimum phase-waveform condition for the L-ray model, which is essentially the same as the one for the two-ray model.

Like the two-ray model, a convex phase-waveform is considered optimum also for the L-ray model. Equation(III40) cannot be strictly satisfied also for the L-ray model. However, if each $\Phi_{\alpha\beta}(\varepsilon,\tau)$ is a strictly monotone increasing/decreasing function as to ε for any τ in $0<\tau<T$, which effectively minimizes each $|F_{\alpha\beta}(\tau)|$ while keeping $\partial\Phi_{\alpha\beta}/\partial\varepsilon$ small

(i.e., keeping the instantaneous frequency deviation due to imposed phase-variation in the timeslot small; cf. Eq.(III23)), then, Eq.(III40) is asymptotically satisfied by increasing its range. Thus, a convex phase-waveform ϕ can asymptotically satisfy the optimum phase-waveform condition in Eq.(III40) by increasing its peak, because the choice of a strictly monotone function for each $\Phi_{\alpha\beta}$ is equivalent to the choice of a convex function for ϕ (cf. Eq.(III22)).

IV NUMERICAL EVALUATION

IV.1 Outline of the Calculation Process

The complex envelope $z_1(t)$ of the received signal including bandpass noise $n(t)$, which is a zero-mean complex gaussian random process in the equivalent low-pass system, is expressed as

$$z_1(t) = \sum_{l=1}^{L} s_l(t) v(t - \tau_l) + n(t) \ . \tag{IV1}$$

On the other hand, Eq.(II5) is rewritten as

$$d(t) = \frac{1}{4}(z_1 z_2^* + z_1^* z_2) = \frac{1}{8}(u_1 u_1^* - u_2 u_2^*) \tag{IV2}$$

by defining u_1 and u_2 as

$$\begin{cases} u_1(t) &= z_1(t) + z_2(t) \\ u_2(t) &= z_1(t) - z_2(t) \end{cases} \ . \tag{IV3}$$

Furthermore, by defining h_i, $u_{1,i}$, $u_{2,i}$, vector $\boldsymbol{u}$, and diagonal matrix $\boldsymbol{H}$ as

$$\begin{cases} h_i &= h(i \cdot t_\Delta) \\ u_{1,i} &= u_1(t_s + i \cdot t_\Delta) \quad ; i = -K, \cdots, 0, \cdots, K \\ u_{2,i} &= u_2(t_s + i \cdot t_\Delta) \end{cases} \tag{IV4}$$

$$\begin{cases} \boldsymbol{u} &= [u_{1,-K}, u_{2,-K}, u_{1,-K+1}, u_{2,-K+1}, \cdots, u_{1,K}, u_{2,K}]^t \\ \boldsymbol{H} &= \mathrm{diag}[h_K, -h_K, h_{K-1}, -h_{K-1}, \cdots, h_{-K}, -h_{-K}] \end{cases} , \tag{IV5}$$

where t_Δ denotes a short interval and ^{t} denotes transpose, from Eq.(II6), the sampled detected signal q is expressed as

$$q = Q(t_s) = \sum_{i=-K}^{K} \frac{h_{-i}}{8}(u_{1,i} u_{1,i}^* - u_{2,i} u_{2,i}^*) = \frac{1}{8} \boldsymbol{u}^\dagger \boldsymbol{H} \boldsymbol{u} \ , \tag{IV6}$$

where † denotes conjugate transpose.

The probability density function $p(q)$ of the sampled signal q, which is expressed as a quadratic form of zero-mean gaussian variables (Eq.(IV6)), is easily obtained by using its characteristic function as shown in Appendix G. The results of $p(q)$ (Eq.(G39) in Appendix G) is expressed by using eigenvalues λ_k of matrix $\boldsymbol{R}^*\boldsymbol{H}$, where the matrix $\boldsymbol{R}$ denotes a covariance matrix expressed, by using $\langle \boldsymbol{u} \rangle$=0 (zero vector), as

$$\boldsymbol{R} = \langle (\boldsymbol{u} - \langle \boldsymbol{u} \rangle)(\boldsymbol{u} - \langle \boldsymbol{u} \rangle)^\dagger \rangle = \langle \boldsymbol{u}\boldsymbol{u}^\dagger \rangle \ , \tag{IV7}$$

and its elements are calculated as shown in Appendix F.

Finally, by means of integration, decision error-rate for mark and space is derived as

$$\begin{cases} P_{e(mark)} = \displaystyle\int_{-\infty}^{0} p(q)dq = \sum_{\lambda_m<0} \frac{1}{\displaystyle\prod_{\substack{n \\ n\neq m}} (1 - \frac{\lambda_n}{\lambda_m})} \\ P_{e(space)} = \displaystyle\int_{0}^{\infty} p(q)dq = \sum_{\lambda_m>0} \frac{1}{\displaystyle\prod_{\substack{n \\ n\neq m}} (1 - \frac{\lambda_n}{\lambda_m})} \end{cases} . \tag{IV8}$$

Because a single decision error causes a single bit error in the Gray encoded system, BER is calculated by simply averaging $P_{e(mark)}$ and $P_{e(space)}$ for occurrence probabilities of mark, space, and adjacent symbol patterns interfering with the current timeslot.

IV.2 Conditions for Calculation

As for phase-waveforms, the stepped type in Eq.(III24), the parabolic (convex) type in Eq.(III26) and ϕ=const., which is equivalent to conventional DPSK, are chosen.

As for postdetection filters, the integrate-and-dump (Eq.(IV9)) and the gaussian (Eq.(IV10)) filters are chosen.

$$h(t)_{I\&D} = \begin{cases} 0 & ; t < -\dfrac{\eta T}{2} \ \ or \ \ t > \dfrac{\eta T}{2} \\ \dfrac{1}{\eta T} & ; -\dfrac{\eta T}{2} \leq t \leq \dfrac{\eta T}{2} \end{cases} \tag{IV9}$$

$$h(t)_{gaussian} = \sqrt{\frac{2\pi}{\ln 2}} B \exp(-\frac{2\pi^2 B^2 t^2}{\ln 2}) \ , \tag{IV10}$$

where $\eta_{\ (symbol)}$ denotes integration interval and B denotes bandwidth.

As for the propagation model, mainly the two-ray Rayleigh fading model with the same average ray power (ρ=1) is chosen and additionally the 1-ray (frequency-nonselective) or 3-ray (each ray has the same average power, i.e., ξ_1=ξ_2=ξ_3) Rayleigh fading model is used for comparison. For the numerical evaluation, maximum Doppler frequency f_D, which the analytical approach cannot deal with, is newly added to the propagation parameters.

IV.3 Results of Calculation

The numerical evaluation results nicely confirm the analytical approach results as shown in Figures IV1 and IV2 compared with Figures III4 and III5. In particular, PSK-VP with a convex phase-waveform is verified as having excellent performance though the delay difference upper limits are slightly reduced.

The reduction of the delay difference upper limit is due to the fact that the ineffective detected signal, which is ignored in the analytical approach, tends to be mixed in the integral interval of the postdetection filter as Region:a is shortened by a long τ. The reduction can be eased by using a postdetection filter with a shorter response settling time. The reduction is eased by using integrate-and-dump filters with a shorter η or a gaussian filter, though the BER for short τ is slightly degraded (Fig.IV3).

The reduction, as shown in Fig.IV4, tends to be accelerated for QPSK-VP, in particular, when using a long η integrate-and-dump postdetection filter. QPSK-VP with a gaussian postdetection filter performs better.

However, the delay difference upper limit is nearly doubled for QPSK-VP as measured in bits. Namely, the upper limit for QPSK-VP with a convex phase-waveform using a gaussian postdetection filter is about 1.7 bits (0.85 symbols, Fig.IV4) in contrast to 0.9 bits for BPSK-VP (Fig.IV3).

As predicted in the analytical approach, BER for PSK-VP on two-ray/three-ray Rayleigh (frequency-selective) fading is remarkably improved by the diversity effect proportional to the square/cube of the SNR, in contrast to directly proportional to the SNR for conventional DPSK on Rayleigh (frequency-nonselective) fading (solid lines in Fig.IV5). As shown in Figures IV4 and IV5, for multipath fading, whose delay differences are less than the delay difference upper limit, PSK-VP shows much better performance than conventional DPSK.

Furthermore, PSK-VP maintains its excellent performance even for rapid fading. As shown in dotted lines in Fig.IV5, the diversity effect can also remarkably decrease the *irreducible error* due to random FM[16]. The irreducible error rate is less than 10^{-4} for quite rapid fading $f_D T$=0.02.

V CONCLUSIONS

The analytical approach based on the diversity with a continuous branch has revealed the major PSK-VP features. The analysis gives us not only physical views such as the

effective order of diversity or equivalency to a path diversity, but also a formula-type BER expression which can estimate the major features including the optimum phase-waveform condition to achieve the best BER, i.e., the ideal boundary for improved BER.

A convex phase-waveform is considered to be optimum, because it approaches the optimum phase-waveform condition asymptotically as its phase shift peak is increased, and effectively while keeping the instantaneous frequency deviation in the timeslot small. PSK-VP with a convex phase-waveform raises the delay difference upper limit to almost 1 symbol.

The numerical evaluation has confirmed the features suggested by the analytical approach. It has also confirmed that 4-ary PSK-VP (QPSK-VP) can nearly double the delay difference upper limit as measured in bits, which is about 1.7 bits for convex phase-waveform. BER of QPSK-VP with a convex phase-waveform is remarkably improved for multipath fading, whose delay difference is less than the upper limit, as compared with conventional DPSK.

The numerical evaluation has additionally revealed not only the influence of the selection for the post-detection filter, but also the robust feature for rapid fading. The irreducible error-rate is less than 10^{-4} even for quite rapid fading $f_D T$=0.02.

Appendix A

Derivation of Detection Output for Two- and L-ray Models

Fading is so slow compared with symbol rate that

$$s_l(t) = s_l(t-T) = s_l \qquad ;1,2 \text{ or } 1,2,\cdots,L \ . \tag{A1}$$

For the two-ray model, Eq.(III1) and Eq.(II4) result in

$$\begin{cases} z_1(t) &= s_1 v(t) + s_2 v(t-\tau) \\ z_2(t) &= s_1 v(t-T)e^{-j\psi} + s_2 v(t-\tau-T)e^{-j\psi} \end{cases} \tag{A2}$$

by using Eq.(A1), respectively. On the other hand, in Region:a, from Eq.(II1)–(II3),

$$\begin{cases} v(t) &= e^{j(\phi(\varepsilon+\tau)+\vartheta_m)} \\ v(t-T) &= e^{j(\phi(\varepsilon+\tau)+\vartheta_m-\theta_m)} \\ v(t-\tau) &= e^{j(\phi(\varepsilon)+\vartheta_m)} \\ v(t-\tau-T) &= e^{j(\phi(\varepsilon)+\vartheta_m-\theta_m)} \end{cases} \tag{A3}$$

are derived by considering $mT \leq t-\tau < (m+1)T$. Then, by using Eq.(II5) additionally, $d_m(\varepsilon)$ is expressed as

$$d_m(\varepsilon) = \frac{1}{2}\cos(\theta_m + \psi) \mid s_1 e^{j\phi(\varepsilon+\tau)} + s_2 e^{j\phi(\varepsilon)} \mid^2 \ . \tag{A4}$$

Consequently, by noting that

$$\frac{1}{2}\cos(\theta_m + \psi) = \frac{1}{2}\mu a_m \ , \tag{A5}$$

we obtain Eq.(III3). Similarly, in Region:b, by considering $(m-1)T \leq t-\tau < mT$,

$$\begin{cases} v(t) &= e^{j(\phi(\varepsilon+\tau)+\vartheta_m)} \\ v(t-T) &= e^{j(\phi(\varepsilon+\tau)+\vartheta_m-\theta_m)} \\ v(t-\tau) &= e^{j(\phi(\varepsilon+T)+\vartheta_{m-1})} \\ v(t-\tau-T) &= e^{j(\phi(\varepsilon+T)+\vartheta_{m-1}-\theta_{m-1})} \end{cases}$$

are derived from Eq.(II1)–(II3). Then, by using Eq.(II5) additionally, $d_m(\varepsilon)$ is expressed as

$$d_m(\varepsilon) = \frac{1}{2}\{\cos(\theta_m + \psi) \mid s_1 \mid^2 + \cos(\theta_{m-1} + \psi) \mid s_2 \mid^2\} \tag{A6}$$

$$+ \cos(\frac{\theta_m + \theta_{m-1}}{2} + \psi)\Re[s_1 s_2^* \exp j(\phi(\varepsilon+\tau) - \phi(\varepsilon+T) + \frac{\theta_m + \theta_{m-1}}{2})] \ .$$

Consequently, by using Eq.(A5), we obtain Eq.(III4).

For the L-ray model, Eq.(A2) is rewritten as

$$\begin{cases} z_1(t) &= \sum_{l=1}^{L} s_l v(t-\tau_l) \\ z_2(t) &= \sum_{l=1}^{L} s_l v(t-\tau_l-T)e^{-j\psi} \end{cases} . \tag{A7}$$

Then, in Region:a, because Eq.(A3) is rewritten as

$$\begin{cases} v(t-\tau_l) &= e^{j(\phi(\varepsilon+\tau-\tau_l)+\vartheta_m)} \\ v(t-\tau_l-T) &= e^{j(\phi(\varepsilon+\tau-\tau_l)+\vartheta_m-\theta_m)} \end{cases} ,$$

from Eq.(II5), $d_m(\varepsilon)$ is expressed as

$$d_m(\varepsilon) = \frac{1}{2}\cos(\theta_m+\psi) \mid \sum_{l=1}^{L} s_l e^{j\phi(\varepsilon+\tau-\tau_l)} \mid^2 .$$

Consequently, by using Eq.(A5), we obtain Eq.(III30).

Appendix B

Analytical Approach Error-rate Derivation for Two- and L-ray Rayleigh Fadings

Because $n\times n$ matrices $\boldsymbol{X}$ and $\boldsymbol{X}_0$ are Hermitian, their eigenvalues λ_i and $\hat{\lambda}_i$ $(i = 1, 2, \cdots, n)$ are real and have the following relationship:

$$\lambda_i = \frac{(1-\tau/T)\Gamma}{n}\hat{\lambda}_i \quad ; \; i = 1, 2, 3, \cdots, n . \tag{B8}$$

For two-ray Rayleigh fading, from rank$\boldsymbol{X}$=rank$\boldsymbol{X}_0\leq$2, non-zero eigenvalues are not greater than two, i.e., $\lambda_3 \sim \lambda_n = 0$ and $\hat{\lambda}_3 \sim \hat{\lambda}_n = 0$. Then, using Eq.(B8)

$$\det(\boldsymbol{I}+\boldsymbol{X}) = \prod_{k=1}^{n}(\lambda_k+1) = (\lambda_1+1)(\lambda_2+1)$$

$$= \{\frac{(1-\frac{\tau}{T})\Gamma}{n}\}^2\hat{\lambda}_1\hat{\lambda}_2 + \frac{(1-\frac{\tau}{T})\Gamma}{n}(\hat{\lambda}_1+\hat{\lambda}_2)+1 . \tag{B9}$$

Consequently, because $\hat{\lambda}_1+\hat{\lambda}_2$ and $\hat{\lambda}_1\hat{\lambda}_2$ result in Eq.(C22) (Appendix C), by using Eq.(B9), Eq.(III10) results in Eq.(III16).

The above derivation is extended to the case of L-ray Rayleigh fading as follows. From rank$\boldsymbol{X}$=rank$\boldsymbol{X}_0 \leq L$, non-zero eigenvalues are not greater than L, i.e., $\lambda_{L+1} \sim \lambda_n = 0$ and $\hat{\lambda}_{L+1} \sim \hat{\lambda}_n = 0$. Then, using Eq.(B8),

$$\det(\boldsymbol{I}+\boldsymbol{X}) = \prod_{k=1}^{n}(\lambda_k+1) = \prod_{k=1}^{L}(\lambda_k+1) = \prod_{k=1}^{L}\{\frac{(1-\frac{\tau}{T})\Gamma}{n}\hat{\lambda}_k+1\} \ .$$

If SNR Γ is high ($\Gamma \gg 1$) and rank$\boldsymbol{X}$=rank$\boldsymbol{X}_0$=L, then,

$$\det(\boldsymbol{I}+\boldsymbol{X}) \approx \{\frac{(1-\frac{\tau}{T})\Gamma}{n}\}^L \prod_{k=1}^{L}\hat{\lambda}_k = \{(1-\frac{\tau}{T})\Gamma\}^L \prod_{k=1}^{L}\xi_k \det \boldsymbol{F} \qquad \text{(B10)}$$

is obtained, as shown in Appendix C, by using $L \times L$ matrix $\boldsymbol{F}$, whose $\alpha\beta$-element is $F_{\alpha\beta}$ in Eq.(C20). Consequently, using Eq.(B10), Eq.(III10) results in Eq.(III36).

Appendix C

Eigenvalues of Matrix $\boldsymbol{X}_0$ for Two- and L-ray Models

First, the derivation is generally done for the L-ray model including the two-ray model as the specific case (i.e., L=2, τ_1=0 and τ_2=τ).

By using matrices $\boldsymbol{X}_l$ whose ik-elements $X_{l,ik}$ are

$$X_{l,ik} = e^{j(\phi_{li}-\phi_{lk})} \quad ; \ l=1,\cdots,L \ , \ i,k=1,2,\cdots,n \ , \qquad \text{(C11)}$$

$\boldsymbol{X}_0$ is expressed as the following linear combination:

$$\boldsymbol{X}_0 = \sum_{l=1}^{L}\xi_l \boldsymbol{X}_l \ . \qquad \text{(C12)}$$

Because rank$\boldsymbol{X}_l$=1, each $\boldsymbol{X}_l$ has only one non-zero eigenvalue, which is n. That is,

$$\boldsymbol{X}_l \boldsymbol{y}_l = n\boldsymbol{y}_l \quad ; \ l=1,\cdots,L \ , \qquad \text{(C13)}$$

where each $\boldsymbol{y}_l$ is the corresponding eigenvector:

$$\boldsymbol{y}_l = [e^{j\phi_{l1}}, e^{j\phi_{l2}}, e^{j\phi_{l3}}, \cdots, e^{j\phi_{ln}}]^t \quad ; \ l=1,\cdots,L \ . \qquad \text{(C14)}$$

On the other hand, there are relationships:

$$\boldsymbol{X}_\alpha \boldsymbol{y}_\beta = \sum_{k=1}^{n} e^{j(\phi_{\beta k}-\phi_{\alpha k})}\boldsymbol{y}_\alpha = \sum_{k=1}^{n} e^{j\Phi_{\alpha\beta k}}\boldsymbol{y}_\alpha \quad ; \ \alpha,\beta=1,\cdots,L \ , \qquad \text{(C15)}$$

where $\Phi_{\alpha\beta}(\varepsilon_k,\tau)$ (Eq.(III38)) is abbreviated to $\Phi_{\alpha\beta k}$. Note that Eq.(C13) is included in Eq.(C15), because $\sum_{k=1}^{n} e^{j\Phi_{\alpha\alpha k}}=n$.

Because $\boldsymbol{X}_0$ is expressed by the linear combination of $\boldsymbol{X}_l$s (Eq.(C12)), whose ranks are one, then, rank$\boldsymbol{X}_0 \leq L$. If rank$\boldsymbol{X}_0=L$, each $\boldsymbol{y}_l$ is linearly independent and the eigenvectors corresponding to the non-zero eigenvalues of $\boldsymbol{X}_0$ can be expressed by linear combination $\sum_{l=1}^{L} p_l \boldsymbol{y}_l$. Then, by using Eq.(C12) and Eq.(C15), the following relationship:

$$\boldsymbol{X}_0 \sum_{l=1}^{L} p_l \boldsymbol{y}_l = (\sum_{l=1}^{L} \xi_l \boldsymbol{X}_l)(\sum_{l=1}^{L} p_l \boldsymbol{y}_l) = \sum_{\alpha=1}^{L}\sum_{\beta=1}^{L} \xi_\alpha p_\beta X_\alpha \boldsymbol{y}_\beta = \sum_{\alpha=1}^{L}\sum_{\beta=1}^{L} (\xi_\alpha p_\beta \sum_{k=1}^{n} e^{j\Phi_{\alpha\beta k}}) \boldsymbol{y}_\alpha \tag{C16}$$

is obtained. By comparing the coefficients of $\boldsymbol{y}_l$ on both sides of Eq.(C16), we obtain

$$\xi_l \sum_{\beta=1}^{L} (p_\beta \sum_{k=1}^{n} e^{j\Phi_{l\beta k}}) = \hat{\lambda} p_l \quad ; \; l = 1, \cdots, L \; , \tag{C17}$$

where $\hat{\lambda}$ denotes the eigenvalue of $\boldsymbol{X}_0$. By rewriting Eq.(C17), the following characteristic equation, whose eigenvalue is $\hat{\lambda}$,

$$n\boldsymbol{\Xi}\boldsymbol{F}\boldsymbol{p} = \hat{\lambda}\boldsymbol{p} \tag{C18}$$

is obtained, where the $L \times L$ diagonal matrix $\boldsymbol{\Xi}$ and the vector $\boldsymbol{p}$ are defined as

$$\boldsymbol{\Xi} = \mathrm{diag}[\xi_1, \cdots, \xi_L]$$

$$\boldsymbol{p} = [p_1, \cdots, p_L]^t \; ,$$

and the $\alpha\beta$-elements $\hat{F}_{\alpha\beta}$ of the $L \times L$ matrix $\boldsymbol{F}$ are expressed as

$$\hat{F}_{\alpha\beta} = \frac{1}{n} \sum_{k=1}^{n} e^{j\Phi_{\alpha\beta k}} \quad ; \; \alpha, \beta = 1, \cdots, L \tag{C19}$$

by noting that $\hat{F}_{\alpha\alpha} = 1$.

Furthermore, by considering $(T-\tau)/n = \varepsilon_{i+1} - \varepsilon_i = \Delta\varepsilon$, because

$$\lim_{n\to\infty} \frac{1}{n} \sum_{k=1}^{n} e^{j\Phi_{\alpha\beta k}} = \frac{1}{T-\tau} \lim_{n\to\infty} \sum_{k=1}^{n} e^{j\Phi_{\alpha\beta k}} \frac{T-\tau}{n}$$

$$= \frac{1}{T-\tau} \lim_{n\to\infty} \sum_{k=1}^{n} e^{j\Phi_{\alpha\beta k}} \cdot \Delta\varepsilon = \frac{1}{T-\tau} \int_0^{T-\tau} e^{j\Phi_{\alpha\beta}(\varepsilon,\tau)} d\varepsilon \; ,$$

if $n \to \infty$, then, Eq.(C19) is rewritten as

$$F_{\alpha\beta}(\tau) = \lim_{n\to\infty} \hat{F}_{\alpha\beta} = \frac{1}{T-\tau} \int_0^{T-\tau} e^{j\Phi_{\alpha\beta}(\varepsilon,\tau)} d\varepsilon \quad ; \; \alpha, \beta = 1, \cdots, L \; . \tag{C20}$$

Finally, by considering that $\hat{\lambda}_k$ is an eigenvalue of matrix $n\boldsymbol{\Xi}\boldsymbol{F}$ and using Eq.(III35),

$$\begin{cases} \sum_{k=1}^{L} \hat{\lambda_k} = \mathrm{tr}(n\boldsymbol{\Xi}\boldsymbol{F}) = n\sum_{k=1}^{L} \xi_k = n \\ \prod_{k=1}^{L} \hat{\lambda_k} = \det(n\boldsymbol{\Xi}\boldsymbol{F}) = n^L \prod_{k=1}^{L} \xi_k \det \boldsymbol{F} \end{cases} \tag{C21}$$

are obtained by noting that all diagonal elements of $\boldsymbol{F}$ are 1.

In particular, for the two-ray model (L=2, τ_1=0, and τ_2=τ), Eq.(C21) is rewritten as

$$\begin{cases} \hat{\lambda}_1 + \hat{\lambda}_2 &= n \\ \hat{\lambda}_1\hat{\lambda}_2 &= \dfrac{\rho}{(1+\rho)^2}(n^2 - \mid F(\tau) \mid^2) \end{cases} \tag{C22}$$

by defining

$$F(\tau) \equiv F_{21}(\tau) = F_{12}(\tau)^* = \frac{1}{T-\tau}\int_0^{T-\tau} e^{j\Phi_{21}(\varepsilon,\tau)}d\varepsilon = \frac{1}{T-\tau}\int_0^{T-\tau} e^{j\Phi(\varepsilon,\tau)}d\varepsilon$$

due to $\Phi_{21}(\varepsilon,\tau) = \Phi(\varepsilon,\tau)$ from Eq.(III14) and Eq.(III38). Note that, if rank$\boldsymbol{X}_0$=1, there is a single non-zero eigenvalue, i.e., $\hat{\lambda}_1$=tr$\boldsymbol{X}_0$=n, then $\hat{\lambda}_2$=0. On the other hand, because r_2=0 in Eq.(III13), ρ=0 or $e^{j\Phi_i}$=const. is obtained. Consequently, Eq.(C22) is also satisfied for rank$\boldsymbol{X}_0$=1.

Appendix D

Proof for Convex Phase-waveform Ensuring L-th Order Diversity Effect in L-ray Model

As shown in Appendix C, because $\boldsymbol{X}_0$ is expressed by the linear combination of $\boldsymbol{X}_l$s (l=1,2,$\cdots$,L) (Eq.(C12)), whose ranks are one, if each eigenvector $\boldsymbol{y}_l$ of $\boldsymbol{X}_l$ corresponding to one non-zero eigenvalue is linearly independent, then, rank$\boldsymbol{X}_0$=L. Then, we will show that each eigenvector is linearly independent for a convex phase-waveform ϕ by the following reductio ad absurdum.

First, we assume that there is a pair of eigenvectors, $\boldsymbol{y}_\alpha$ and $\boldsymbol{y}_\beta$ ($\alpha \neq \beta$) which are not linearly independent, then,

$$\boldsymbol{y}_\alpha = a\boldsymbol{y}_\beta. \tag{D23}$$

where a is a complex constant. From Eq.(C14) and Eq.(III32), by considering $n\rightarrow\infty$, and by replacing a ($|a|$=1) to $e^{j\varphi}$, Eq.(D23) is rewritten as

$$e^{j\phi(\varepsilon+\tau_\alpha)} = ae^{j\phi(\varepsilon+\tau_\beta)} = e^{j\varphi}e^{j\phi(\varepsilon+\tau_\beta)}$$

that is,

$$\phi(\varepsilon+\tau_\alpha)=\phi(\varepsilon+\tau_\beta)+\varphi \quad : \bmod 2\pi. \tag{D24}$$

Because Eq.(D24) is satisfied for any ε in $0<\varepsilon<T-\tau$, if ϕ is a continuous function (if not, then, ϕ cannot be a convex function), by subtracting Eq.(D24) from the same equation where ε is rewritten as $\varepsilon+\delta$ ($0<\delta\ll 1$, $0<\varepsilon<T-\tau-\delta$),

$$\phi(\varepsilon+\tau_\alpha)-\phi(\varepsilon+\delta+\tau_\alpha)=\phi(\varepsilon+\tau_\beta)-\phi(\varepsilon+\delta+\tau_\beta) \tag{D25}$$

is obtained. Equation(D25) is inconsistent with a convex phase-waveform ϕ.

Consequently, each eigenvector $\boldsymbol{y}_l$ (l=1,2,$\cdots$,L) corresponding to one non-zero eigenvalue is linearly independent, that is, rank$\boldsymbol{X}_0$=L.

Appendix E

The BER lower limit for the L-ray Rayleigh Fading

By defining vector $\boldsymbol{\phi}(\varepsilon)$

$$\boldsymbol{\phi}(\varepsilon)=[e^{-j\phi_1(\varepsilon)},e^{-j\phi_2(\varepsilon)},\cdots,e^{-j\phi_L(\varepsilon)}]^t\ ,$$

the matrix $\boldsymbol{F}$ can be also expressed in the style of covariance matrix as follows:

$$\boldsymbol{F}=\frac{1}{T-\tau}\int_0^{T-\tau}\boldsymbol{\phi}(\varepsilon)\boldsymbol{\phi}(\varepsilon)^\dagger d\varepsilon\ .$$

Thus, obviously, the matrix $\boldsymbol{F}$ is Hermitian positive semi-definite, then, its all eigenvalues $\tilde{\lambda}_k$ (k=1,2,$\cdots$,L) are positive or zero. Consequently, by using the relationship between arithmetic mean and geometric mean,

$$\sqrt[L]{\det\boldsymbol{F}}=\sqrt[L]{\prod_{k=1}^{L}\tilde{\lambda}_k}\le\frac{\sum_{k=1}^{L}\tilde{\lambda}_k}{L}=\frac{\mathrm{tr}\boldsymbol{F}}{L}=\frac{L}{L}=1\ ,$$

that is, the relationship:

$$0<\det\boldsymbol{F}\le 1 \tag{E26}$$

is obtained. On the other hand, all ξ_l (Eq.(III35)) are also positive or zero, then, by using the relationship between arithmetic mean and geometric mean,

$$\sqrt[L]{\prod_{k=1}^{L}\xi_k}\le\frac{\sum_{k=1}^{L}\xi_k}{L}=\frac{1}{L}\ ,$$

that is, the relationship:

$$0 < \prod_{k=1}^{L} \xi_k \leq \frac{1}{L^L} \tag{E27}$$

is obtained. From Eq.(E26) and Eq.(E27), Eq.(III39) is obtained as the lower limit of the right-hand term of Eq.(III36).

The equality condition of Eq.(III39) is derived from equality conditions of Eq.(E26) and Eq.(E27). Because the equality condition in Eq.(E26) is $\forall\tilde{\lambda}_k$=1, i.e., matrix $\boldsymbol{F}$ is diagonal (diagonal elements are 1), then, Eq.(III40) is obtained. On the other hand, because the equality condition in Eq.(E27) is equality of all ξ_k, then Eq.(III41) is obtained.

Appendix F

Calculation of the covariance matrix $\boldsymbol{R}$

The 2×2 partitioned matrix R_{ik} $(i, k{=}-K, \cdots, K)$ of the covariance matrix $\boldsymbol{R}$ is written as

$$R_{ik} = \begin{bmatrix} \langle u_{1,i} u_{1,k}^* \rangle & \langle u_{1,i} u_{2,k}^* \rangle \\ \langle u_{2,i} u_{1,k}^* \rangle & \langle u_{2,i} u_{2,k}^* \rangle \end{bmatrix} = \begin{bmatrix} A+B+C+D & A-B-C+D \\ A-B+C-D & A+B-C-D \end{bmatrix} \tag{F28}$$

from Eq.(IV5), Eq.(IV7) and Eq.(IV3), where

$$\begin{cases} A = \langle z_{1,i} z_{1,k}^* \rangle \quad , \quad B = \langle z_{2,i} z_{2,k}^* \rangle \\ C = \langle z_{1,i} z_{2,k}^* \rangle \quad , \quad D = \langle z_{2,i} z_{1,k}^* \rangle \end{cases} \tag{F29}$$

by abbreviating $z_1(t_s + i \cdot t_\Delta)$ and $z_2(t_s + i \cdot t_\Delta)$ to $z_{1,i}$ and $z_{2,i}$, respectively.

If there is no correlation between each fading and between the signal and noise, i.e.,

$$\langle s_i(t_1) s_k^*(t_2) \rangle = \begin{cases} 0 & ; i \neq k \\ \sigma_{sl}^2 \rho_{sl}(t_1 - t_2) & ; i = k = l \end{cases} \tag{F30}$$

$$\langle s_l(t) v(t - \tau_l) \cdot n^*(t) \rangle = 0 \tag{F31}$$

$$\langle n(t_1) n^*(t_2) \rangle = \sigma_n^2 \rho_n(t_1 - t_2) \tag{F32}$$

by calculating Eq.(F29) using the above relationships, A, B, C, and D in Eq.(F28) are

expressed as

$$\begin{cases} A = & \sum_{l=1}^{L} \sigma_{sl}^2 \rho_{sl}(\overline{i-k} \cdot t_\Delta) e^{j\{\zeta(t_{l1i})-\zeta(t_{l1k})\}} & + & \sigma_n^2 \rho_n(\overline{i-k} \cdot t_\Delta) \\ B = & \sum_{l=1}^{L} \sigma_{sl}^2 \rho_{sl}(\overline{i-k} \cdot t_\Delta) e^{j\{\zeta(t_{l2i})-\zeta(t_{l2k})\}} & + & \sigma_n^2 \rho_n(\overline{i-k} \cdot t_\Delta) \\ C = & \sum_{l=1}^{L} \sigma_{sl}^2 \rho_{sl}(\overline{i-k} \cdot t_\Delta + T) e^{j\{\zeta(t_{l1i})-\zeta(t_{l2k})+\psi\}} & + & \sigma_n^2 \rho_n(\overline{i-k} \cdot t_\Delta + T) \\ D = & \sum_{l=1}^{L} \sigma_{sl}^2 \rho_{sl}(\overline{i-k} \cdot t_\Delta - T) e^{j\{\zeta(t_{l2i})-\zeta(t_{l1k})-\psi\}} & + & \sigma_n^2 \rho_n(\overline{i-k} \cdot t_\Delta - T) \end{cases} , \quad \text{(F33)}$$

where

$$\begin{cases} t_{l1i} &= t_s + i \cdot t_\Delta - \tau_l \\ t_{l1k} &= t_s + k \cdot t_\Delta - \tau_l \\ t_{l2i} &= t_s + i \cdot t_\Delta - \tau_l - T \\ t_{l2k} &= t_s + k \cdot t_\Delta - \tau_l - T \end{cases} , \quad \text{(F34)}$$

and $\sigma_{sl}^2/2$ and $\rho_{sl}(t)$ in Eq.(F30) are the power and the autocorrelation function of the l-th path, respectively. $\sigma_n^2/2$ and $\rho_n(t)$ in Eq.(F32) are the power and the autocorrelation function of the noise, respectively. In this paper, a nondirectional receiving antenna and constant mobile speed are assumed. Then, $\rho_{sl}(t)$ is expressed as [17]

$$\rho_{sl}(t) = J_0(2\pi f_D t) , \quad \text{(F35)}$$

where f_D is maximum Doppler frequency. On the other hand, the predetection bandpass filter is assumed to be a rectangular filter with bandwidth B_N (in this paper, $B_N T$=2.0 is used), which is wide enough not to distort the PSK-VP signal, then

$$\rho_n(t) = \sin(\pi B_N t)/(\pi B_N t) . \quad \text{(F36)}$$

Appendix G

Derivation of the probability density function $p(q)$

To obtain the probability density function $p(q)$, first, we obtain its characteristic function $G(\xi)$ defined as

$$G(\xi) \equiv \int_{-\infty}^{\infty} p(q) e^{j\xi q} dq .$$

$G(\xi)$ can be expressed in Eq.(G37) for a quadratic form of zero-mean gaussian variables such as Eq.(IV6)[12],

$$G(\xi) = \frac{1}{\det(\boldsymbol{I} - 2j\xi \boldsymbol{R}^* \boldsymbol{H})} = \frac{1}{\prod_k (1 - 2j\xi\lambda_k)} , \tag{G37}$$

where $\boldsymbol{R}$ denotes covariance matrix of $\boldsymbol{u}$ (Eq.(IV7)) and λ_k are eigen values of matrix $\boldsymbol{R}^*\boldsymbol{H}$.

Then, by means of inverse Fourier transformation, i.e.,

$$p(q) = \frac{1}{2\pi} \int_{-\infty}^{\infty} G(\xi) e^{-j\xi q} d\xi , \tag{G38}$$

$p(q)$ is obtained. Consequently, by calculating Eq.(G38) using the residue theorem, the probability density function $p(q)$ is expressed as

$$p(q) = \begin{cases} \displaystyle\sum_{\lambda_m > 0} \frac{1}{2\lambda_m} \cdot \frac{e^{-\frac{q}{2\lambda_m}}}{\displaystyle\prod_{\substack{n \\ n \neq m}} (1 - \frac{\lambda_n}{\lambda_m})} & ; q > 0 \\ \displaystyle -\sum_{\lambda_m < 0} \frac{1}{2\lambda_m} \cdot \frac{e^{-\frac{q}{2\lambda_m}}}{\displaystyle\prod_{\substack{n \\ n \neq m}} (1 - \frac{\lambda_n}{\lambda_m})} & ; q < 0 \end{cases} . \tag{G39}$$

Acknowledgment

The author wishes to thank Yuhei Mori (NTT) for his helpful suggestions about the eigenvalue analysis in the analytical approach. The author also wishes to express sincere thanks to Yoji Furuhama, Masami Akaike and other staff of ATR Optical and Radio Communications Research Laboratories for their continual encouragements and discussions about this research.

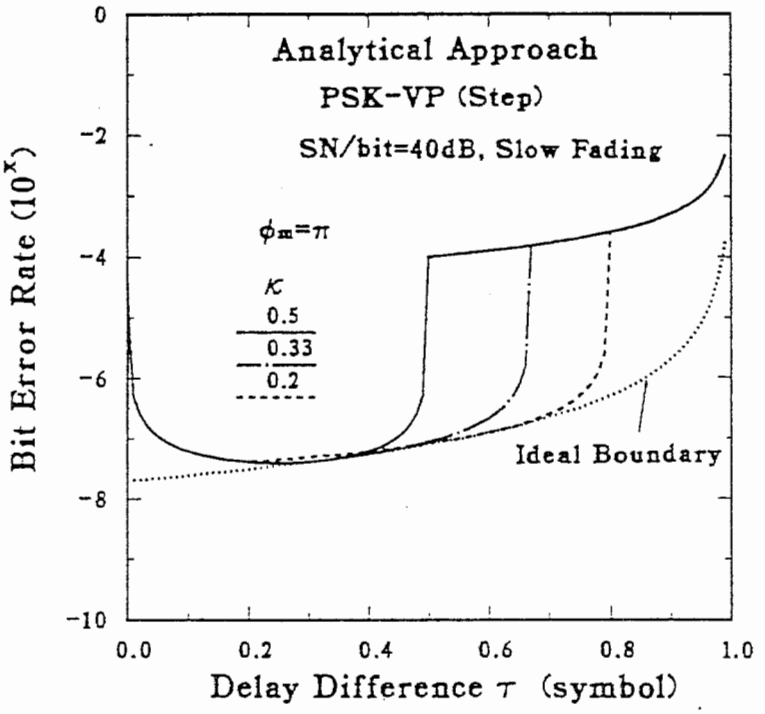

Figure III4. Analytical approach results for 2- or 4-ary PSK-VP with stepped phase-waveforms compared with the ideal boundary in two-ray Rayleigh fading.

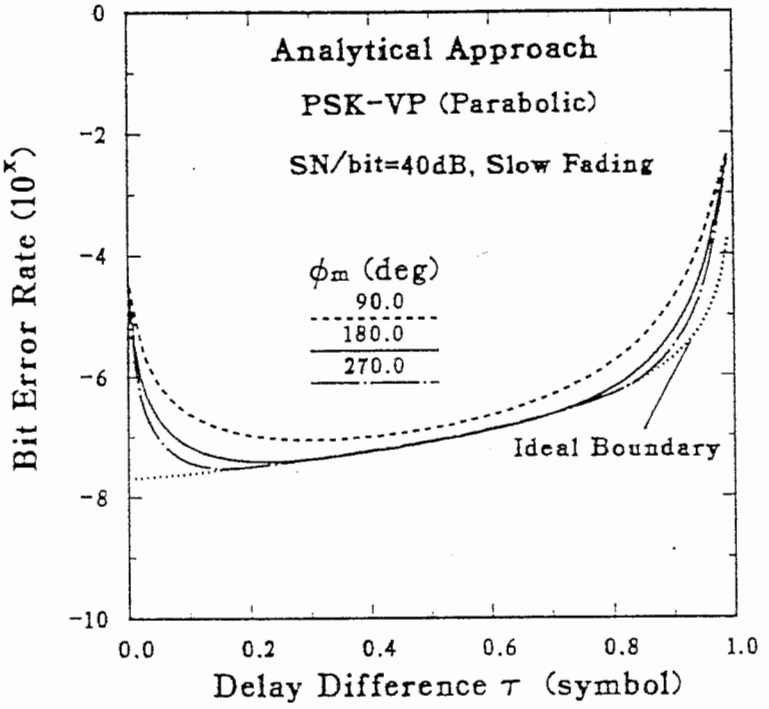

Figure III5. Analytical approach results for 2- or 4-ary PSK-VP with parabolic (convex) phase-waveforms compared with the ideal boundary in two-ray Rayleigh fading.

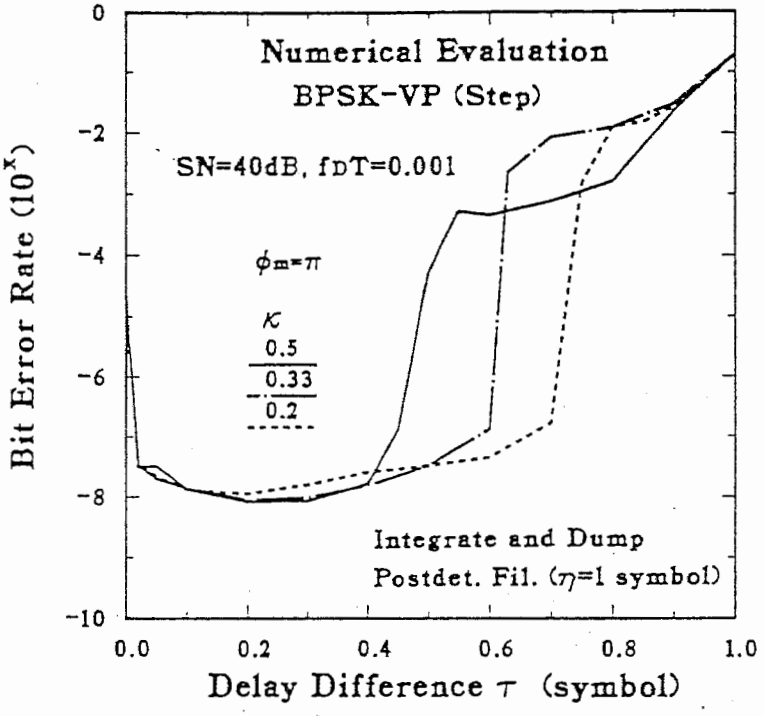

Figure IV1: Numerical evaluation results for BPSK-VP with stepped phase-waveforms.

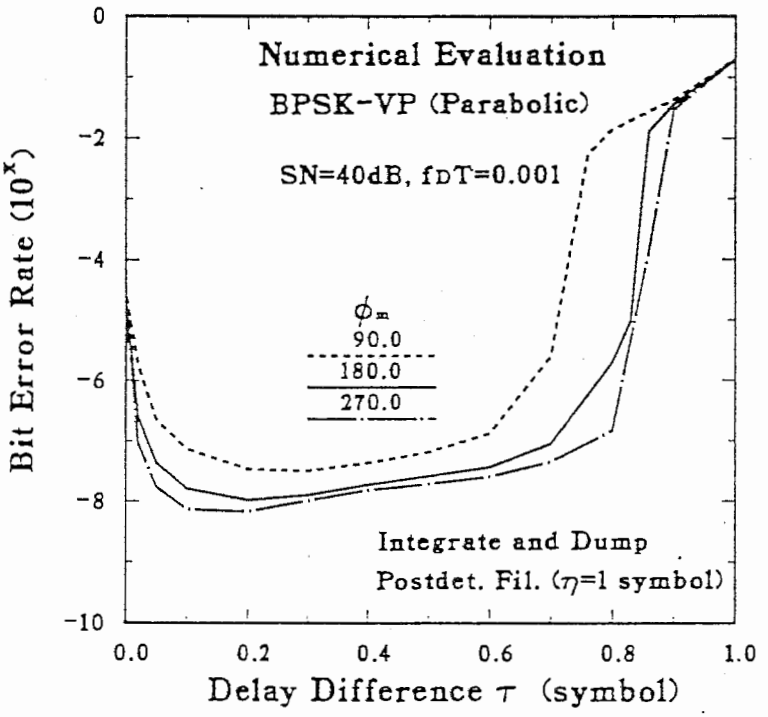

Figure IV2. Numerical evaluation results for BPSK-VP with parabolic (convex) phase-waveforms.

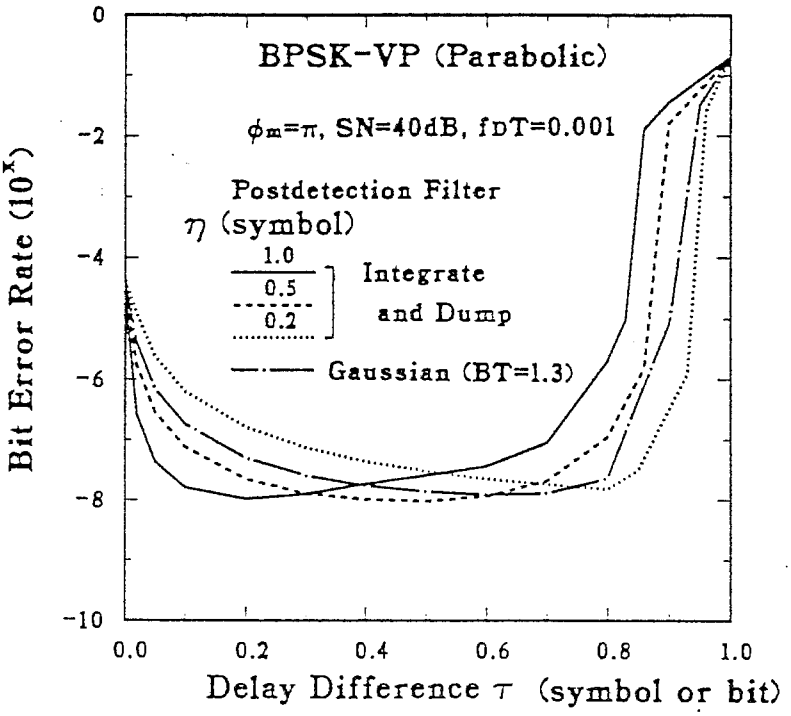

Figure IV3. BER vs. τ performances of BPSK-VP with parabolic (convex) phase-waveform for various postdetection filters in two-ray Rayleigh fading.

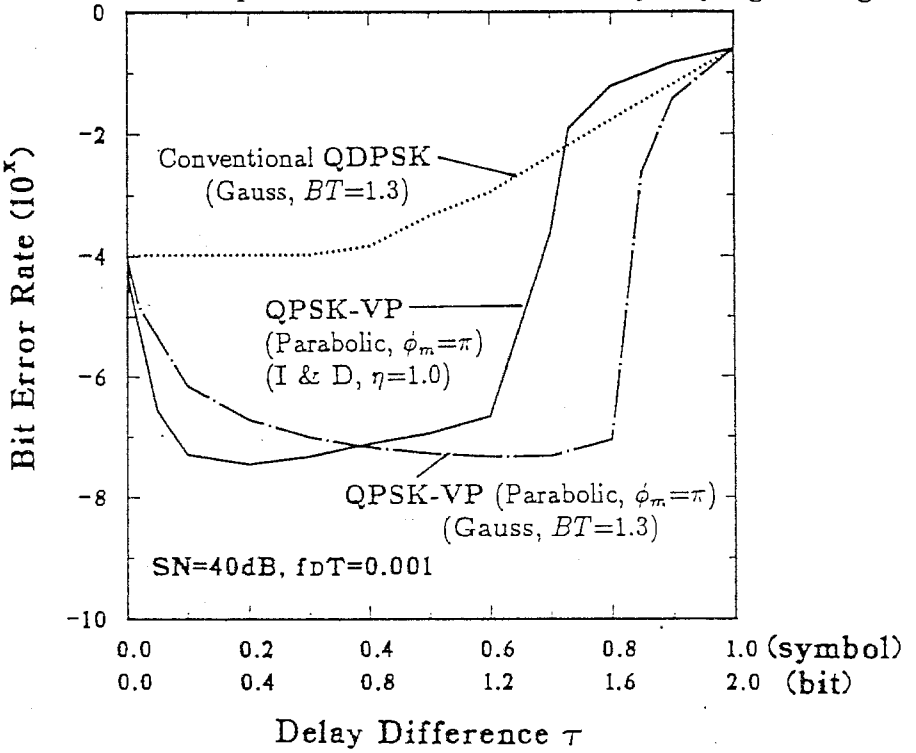

Figure IV4. BER vs. τ performances of QPSK-VP with parabolic (convex) phase-waveform using gaussian postdetection filter compared with QPSK-VP using integrate-and-dump (abbreviated to I & D) and conventional QDPSK in two-ray Rayleigh fading.

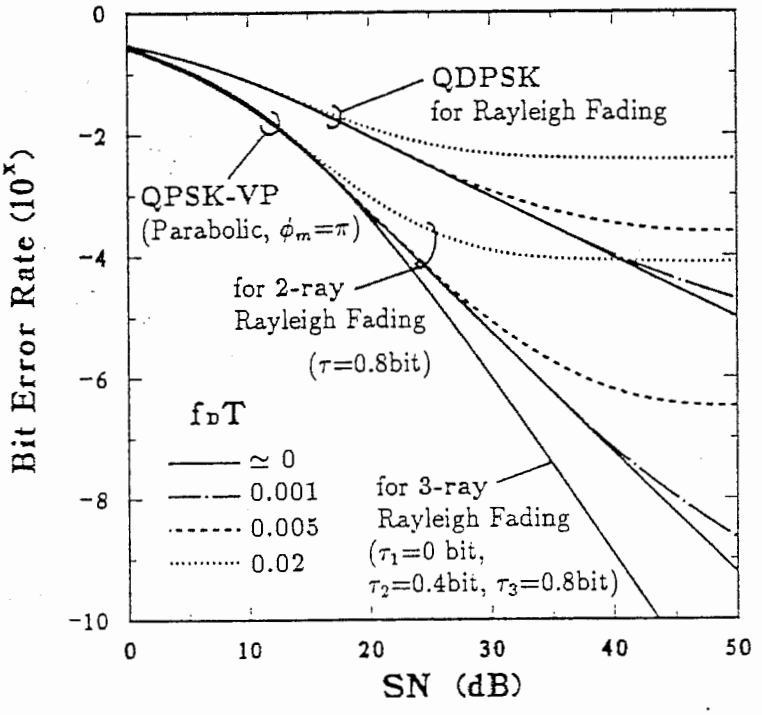

Figure IV5. BER vs. SNR performances of QPSK-VP with parabolic (convex) phase-waveform using gaussian postdetection filter (BT=1.3) in 2- and 3-ray Rayleigh fading for various f_D compared with conventional QDPSK in Rayleigh (frequency-nonselective) fading.

Bibliography

[1] G. L. Turin, F. D. Clapp, T. L. Johnston, S. B. Fine, and D. Lavry, "A statistical model of urban multipath propagation," *IEEE Trans. Veh. Technol.*, vol. VT-21, pp. 1–9, Feb. 1972.

[2] D. C. Cox, "910 MHz urban mobile radio propagation: Multipath characteristics in New York City," *IEEE Trans. Commun.*, vol. COM-21, pp. 1188–1194, Nov. 1973.

[3] D. L. Nielson, "Microwave propagation measurements for mobile digital radio application," *IEEE Trans. Veh. Tech.*, vol. 27, pp. 117–132, Aug. 1978.

[4] P. A. Bello and B. D. Nelin, "The effect of frequency selective fading on the binary error probabilities of incoherent and differentially coherent matched filter receivers," *IEEE Trans. Commun. Syst.*, vol. CS-11, pp. 170–186, June 1963.

[5] J. Horikoshi, "Error performance considerations of $\pi/2$-TFSK under the multipath interfering environment," *Trans. IECE Japan*, vol. E67, No. 1, pp. 40–46, Jan. 1984.

[6] S. Ariyavisitakul, S. Yoshida, F. Ikegami, and T. Takeuchi, "A novel anti-multipath modulation technique DSK," *IEEE Trans. Commun.*, vol. COM-35, No. 12, pp. 1252–1264, Dec. 1987.

[7] S. Ariyavisitakul, S. Yoshida, F. Ikegami, and T. Takeuchi, "A proposal of an anti-multipath modulation technique PSK-RZ," *Papers, Tech. Group Commun.*, IECE Japan, CS85-155, Jan. 1986.

[8] H. Takai, "A proposal of an anti-multipath modulation technique" (in Japanese), *Papers, Tech. Group Commun.*, IECE Japan, CS86-48, Sept. 1986.

[9] S. Yoshida and F. Ikegami, "Anti-multipath modulation technique — Manchester-coded PSK (MC-PSK) —," in *Proc. IEEE ICC'87*, pp. 39.3.1–39.3.5, Seattle, June 1987.

[10] H. Takai, "BER performance of anti-multipath modulation PSK-VP and its optimum phase-waveform," in *Proc. IEEE VTC'90*, pp. 412–419, Orlando, May 1990.

[11] M. Kac and A. J. F. Siegert, "On the theory of noise in radio receivers with square law detectors," *J. Appl. Phys.*, vol. 18, pp. 383–397, Apr. 1947.

[12] G. L. Turin, "The characteristic function of hermitian quadratic forms in complex normal variables," *Biometrika*, vol. 47, pp. 199–201, June 1960.

[13] J. H. Winters, "Differential detection with intersymbol interference and frequency uncertainty," *IEEE Trans. Commun.*, vol. COM-32, No. 1, pp. 25–33, Jan. 1984.

[14] M. Schwartz, W. R. Bennett, and S. Stein, *Communication systems and techniques.* New York: McGraw-Hill, 1966, ch. 10–11.

[15] J. G. Proakis, *Digital communications.* New York: McGraw-Hill, 1983, ch. 7.

[16] W. C. Y. Lee, *Mobile communications engineering.* New York: McGraw-Hill, 1982, ch. 13.

[17] R. H. Clarke, "A statistical theory of mobile radio reception," *Bell Syst. Tech. J.*, vol. 47, pp. 957–1000, July–Aug. 1968.